OPEN ACCESS
Article

Nitrogen isotope constraints on Terreneuvian shallow-marine redox evolution in the Aksu area, Tarim Basin

Shiyan Liu, Zhenfei Wang, Pengcheng Ju and Chao Chang*

***E-mail:** changchao@nwu.edu.cn

Received 2 June 2026; Revised 3 July 2026; Accepted 10 July 2026; Published 4 August 2026

https://doi.org/10.55092/cle20260008

Graphical Abstract

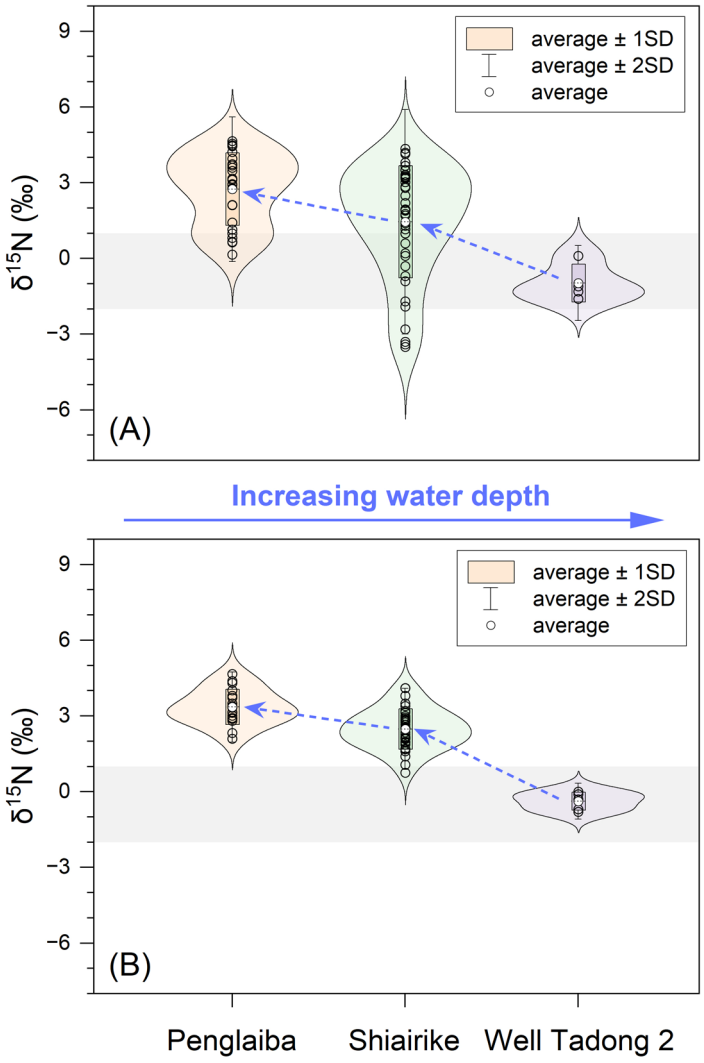

Highlights:

- High-resolution Terreneuvian $\delta^{15}N$ records are documented from the Aksu area, Tarim Basin.
- A two-stage deoxygenation–reoxygenation redox history of the shallow ocean is identified.
- A persistent depth-dependent redox gradient across the basin is demonstrated.

Nitrogen isotope constraints on Terreneuvian shallow-marine redox evolution in the Aksu area, Tarim Basin

Shiyan Liu[1,2], Zhenfei Wang[3], Pengcheng Ju[4] and Chao Chang[1,*]

[1] State Key Laboratory of Continental Evolution and Early Life, Shaanxi Key Laboratory of Early Life and Environment, and Department of Geology, Northwest University, Xi'an 710069, China

[2] Anhui Earthquake Agency, Hefei 230031, China

[3] International Center for Isotope Effects Research, State Key Laboratory of Critical Earth Material Cycling and Mineral Deposits, Nanjing University, Nanjing 210023, China

[4] School of Earth and Space Sciences, University of Science and Technology of China, Hefei 230026, China

***E-mail:** changchao@nwu.edu.cn.

Abstract: The Cambrian Explosion witnessed the rapid radiation of nearly all animal phyla in three distinct evolutionary phases. Recent studies from South China have proposed that the prevalence of suboxic environments in the Terreneuvian shallow ocean facilitated the diversification of lophotrochozoans with relatively low oxygen requirements during the second phase of the Cambrian Explosion. To further test this hypothesis, we present a high-resolution $\delta^{15}N$ record from the inner-ramp Penglaiba section in the Aksu area, Tarim Basin, an independent paleocontinent with exceptionally well-preserved Terreneuvian successions. Our results document a progressive decrease in $\delta^{15}N$ values from > +4‰ to < +1‰ in the lower unit of the Yuertusi Formation, followed by stable $\delta^{15}N$ values of ~+3‰ in the upper unit. This isotopic pattern records a two-stage redox history for the shallow Tarim Basin, with progressive intensification of water-column deoxygenation succeeded by partial reoxygenation. Integrated with published regional $\delta^{15}N$ data, our results demonstrate the existence of a persistent depth-dependent redox gradient throughout the Terreneuvian, with denitrification intensity decreasing systematically from anoxic deep-basin to suboxic inner-ramp environments. These findings provide cross-basin validation for the hypothesis that stepwise oxygenation of the shallow ocean modulated the multi-phase evolutionary trajectory of metazoans during the Cambrian Explosion.

Keywords: Yuertusi Formation; Terreneuvian; nitrogen isotope; suboxic; depth gradient

1. Introduction

The Cambrian Explosion, marked by the rapid emergence of nearly all animal phyla and fundamental transformations of marine ecosystems, represents one of the most consequential biological events in Earth's history (Zhang and Shu 2014, 2021). Three distinct phases of this evolutionary radiation are well documented in the fossil record: the appearance of basal metazoans in the latest Ediacaran, the diversification of lophotrochozoans in the Terreneuvian, and the subsequent rise of ecdysozoans and deuterostomes in Cambrian Age 3 (Shu *et al.* 2014). The Terreneuvian Epoch occupies a pivotal position as it bridges the transition from microbial mat-dominated Precambrian ecosystems to metazoan-dominated Phanerozoic ecosystems (Erwin and Valentine 2013; Zhang and Shu 2014, 2021), making it critical for unraveling the interplay between environmental change and biological evolution during the Cambrian Explosion.

Given that complex metazoan metabolism and behavior require sustained oxygen availability, it has long been hypothesized that rising marine oxygen levels were a key external driver fueling early Cambrian animal diversification (e.g., Sperling *et al.* 2013, 2015; Li *et al.* 2017, 2018; Fan *et al.* 2023). However, accumulating geochemical evidence indicates that the Ediacaran–Cambrian transition was characterized by highly dynamic redox fluctuations rather than a monotonic increase in global ocean oxygenation. For instance, Wei *et al.* (2018) identified a prominent negative excursion in the Terreneuvian carbonate uranium isotope record, which they interpreted as evidence for a substantial expansion of marine anoxia. Subsequent constraints on uranium isotope fractionation under ferruginous conditions suggested that such uranium isotope records may instead reflect variations in the areal extent of euxinic water masses (Cole *et al.* 2020). On the other hand, high-resolution nitrogen isotope studies from the Yangtze Subprovince of South China (Algeo and Li 2026) have documented the widespread occurrence of suboxic, denitrification-dominated conditions in shallow-marine environments during this interval (Chang and Algeo 2025; Zheng *et al.* 2025). Intriguingly, the second phase of the Cambrian Explosion in the Terreneuvian was

Continent and Life Evolution

dominated by lophotrochozoans with relatively low oxygen requirements (Zhang and Cui 2016). As a consequence, it was suggested that the prevailing of low-oxygen shallow-marine environments may have created a unique evolutionary window that facilitated the ecological success of lophotrochozoans (Zheng *et al.* 2025).

This study aims to test global generality of this hypothesis by constraining shallow-marine redox conditions in the Tarim Block, a separate paleocontinent with well-preserved Terreneuvian successions (Zhao *et al.* 2018). While previous nitrogen isotope work from the Tarim Basin has established a redox gradient from middle-ramp to deep-water settings (Zhu *et al.* 2024), the redox conditions of the shallowest inner-ramp environments remain uncharacterized. Here, we fill this critical gap by presenting a high-resolution multi-proxy dataset ($\delta^{15}N$, $\delta^{13}C_{org}$, total organic carbon (TOC), total nitrogen (TN)) from the Penglaiba section in the Aksu area (Figure 1). Our results clarify the redox environment in the inner-ramp facies and complement a more comprehensive reconstruction of Terreneuvian spatial redox heterogeneity in the Tarim Basin. These findings have important implications for understanding the environmental controls on the Cambrian Explosion and the role of oxygen in shaping early animal evolution.

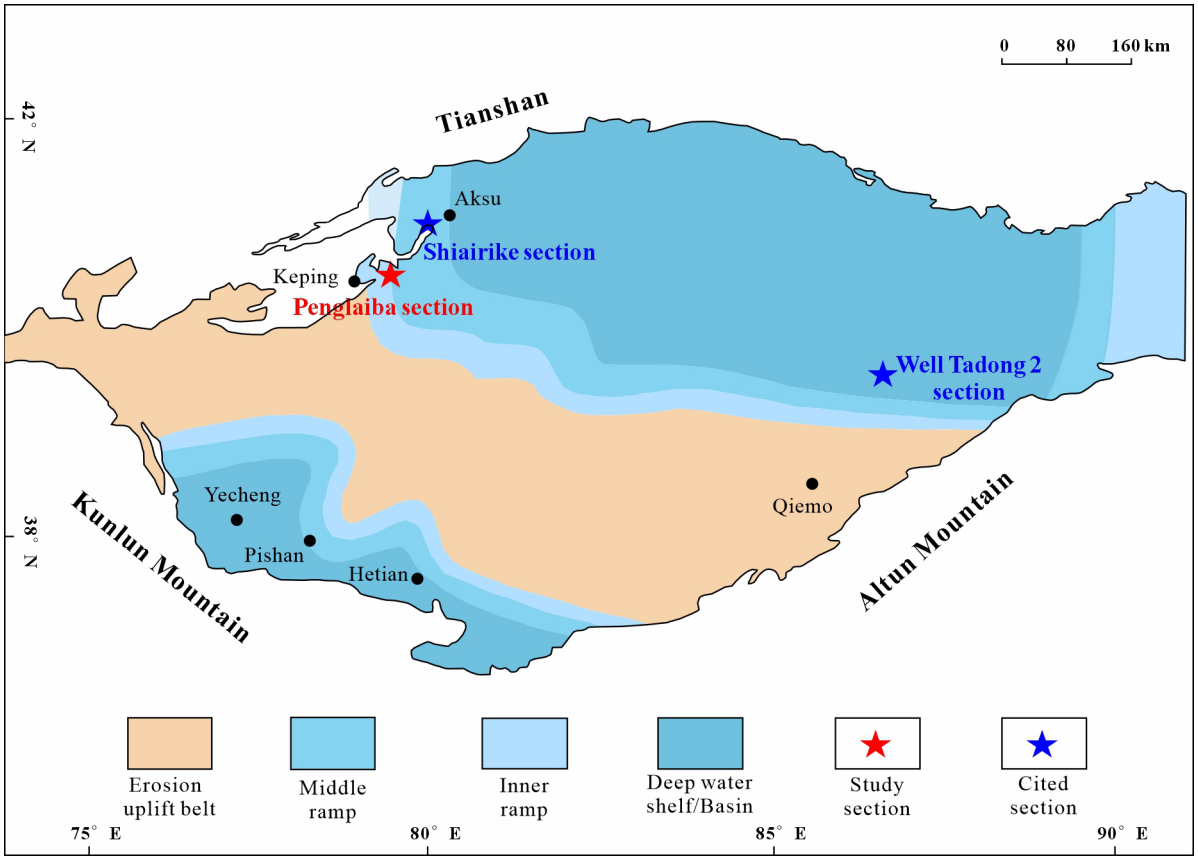

Figure 1. Paleogeographic map of the Tarim Basin during the early Cambrian (after Tian *et al.* 2018).

2. Geologic setting

During the early Cambrian, the Tarim Block evolved into an epicontinental sea (Zhang *et al.* 2013) and was likely positioned at the northwestern margin of Gondwana supercontinent within the equatorial belt (Li *et al.* 2008; Zhao *et al.* 2018). The Tarim Basin developed a topographic gradient with higher elevations in the southwest and lower elevations in the northeast, accompanied by a corresponding facies transition from shallow ramp to deep-shelf and basinal settings (Figure 1). The Aksu area, located on the northwestern margin of the Tarim Basin (Figure 1), preserves a relatively complete lower Cambrian sedimentary succession.

The Yuertusi Formation comprises a succession of highly organic-rich black shales deposited during the widespread marine transgression that marked the onset of the Cambrian (Liu *et al.* 2012; Zhu *et al.* 2021). Previous studies have documented two small shelly fossil (SSF) assemblage zones within the Yuertusi Formation. The basal SSF zone correlates with the lower Cambrian Meishucunian Stage in the Yangtze Subprovince of South China (Yao *et al.* 2005), while the upper SSF zone corresponds to the lower Qiongzhusian Stage (Qian *et al.* 2000; Qian *et al.* 2009). Chemostratigraphic analyses of carbonate carbon isotopes further confirm the presence of BACE (negative excursion at the base of the Cambrian System) in the Yuertusi Formation and CARE (positive excursion near the base of Stage 3) in the overlying Xiaoerbrak Formation (Zhu *et al.* 2006; Guo *et al.* 2017; Zhang *et al.* 2020). Taken together, these

biostratigraphic and chemostratigraphic constraints indicate that the Yuertusi Formation is primarily of Terreneuvian age.

The Penglaiba section investigated in this study is located in southwestern Aksu City. The Yuertusi Formation at this section is ca. 13 m thick and comprises, in ascending order, bedded chert with phosphatic nodules, bedded chert with intercalated black shale, and black shale (Figure 2). Its depositional environment is interpreted as a shallow-water ramp platform (Figure 1). The formation is underlain by the Qigebulak Formation and overlain by the Xiaoerbrak Formation, both dominated by dolostone (Figure 2).

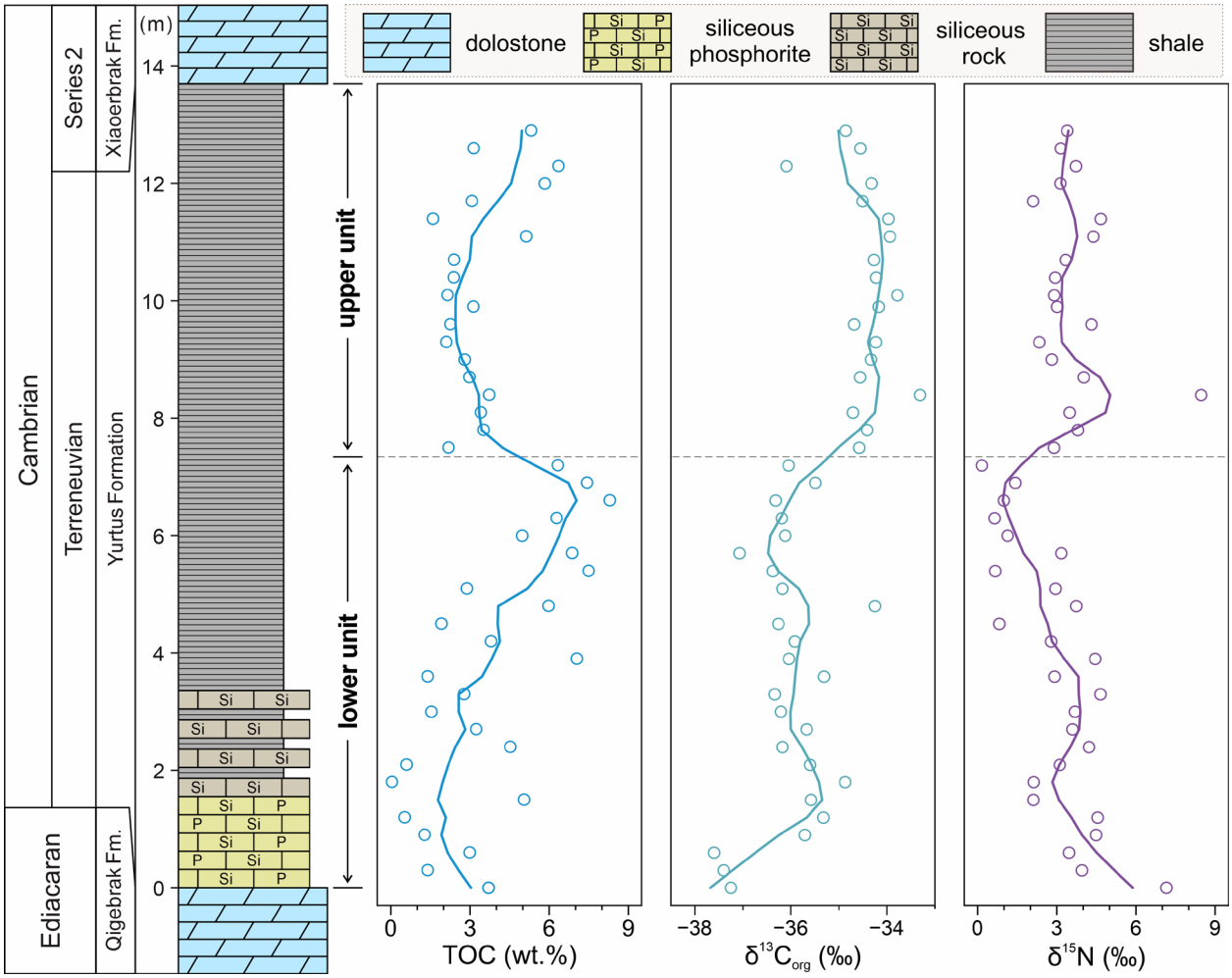

Figure 2. Stratigraphic distributions of TOC, $\delta^{13}C_{org}$, and $\delta^{15}N$ in the Penglaiba section. Solid trend lines are provided by LOWESS curves.

3. Samples and methods

A total of 45 bulk rock samples were systematically collected from the Penglaiba section, covering the complete stratigraphic succession from base to top. To eliminate potential surface contamination, fresh interior fragments were isolated from each sample by mechanical chipping, then pulverized to a 200-mesh grain size for subsequent geochemical measurements.

TOC and TN concentrations were determined by combustion elemental analysis at the Hua-Ke-Jing-Xin Stable Isotope Laboratory. Approximately 20 mg of decalcified sample powder was weighed into tin capsules for analysis using a MACRO Cube Elemental Analyzer (Elementar, Germany). Decalcification was performed by repeated treatment with 1 M HCl at 60 °C until no effervescence was observed, followed by rinsing with Milli-Q water and drying at 60 °C. Analytical precision was monitored using the sulphanilamide reference standard (TOC = 41.81 wt.%; TN = 16.26 wt.%), which was analyzed after every 12 samples. A one-point calibration procedure was employed for quantification. The long-term analytical uncertainties were estimated to be ±0.05 wt.% for TOC and ±0.03 wt.% for TN.

Stable carbon and nitrogen isotopic compositions of the organic fraction were measured at the Third Institute of Oceanography, Ministry of Natural Resources, Xiamen, China. Analyses were performed using a Thermo Finnigan Delta V Advantage isotope ratio mass spectrometer (IRMS). Analytical accuracy and precision were rigorously controlled using two reference materials: an international standard (UREA, IVA33802174: $\delta^{13}C$ = −37.02‰; $\delta^{15}N$ = −2.91‰) and an in-house working standard (Acetanilide #1: $\delta^{13}C$ = −29.53‰; $\delta^{15}N$ = +1.18‰). Prior to each analytical

run, three procedural blanks and three empty tin capsules were analyzed to quantify blank contributions. $\delta^{15}N$ values are reported relative to atmospheric nitrogen (AIR), and $\delta^{13}C$ values are reported relative to the Vienna Pee Dee Belemnite (VPDB) standard. A one-point calibration was used for isotopic ratio calculations. Reference materials were analyzed after every 12 samples. The average within-run reproducibility (1σ) based on replicate reference material measurements was ±0.30‰ for $\delta^{15}N$ and ±0.20‰ for $\delta^{13}C_{org}$. All samples with TN ≤ 0.1 wt.% have been analyzed at least twice to demonstrate fidelity of the analytical results.

4. Results

Geochemical data from the Penglaiba section are summarized in Supplementary Table S1, with vertical profiles of TOC, $\delta^{13}C_{org}$, and $\delta^{15}N$ ratios presented in Figure 2.

Stratigraphic variations in these proxies allow the Yuertusi Formation to be subdivided into two geochemically distinct units (Figure 2). The lower unit consists of siliceous phosphorite, chert, and the lower black shale succession. Within this unit, TOC increases gradually up-section from ~2 wt.% to ~6 wt.%. $\delta^{13}C_{org}$ values remain relatively invariant at ~−36‰ across the entire lower unit, with the exception of a few anomalously depleted values (~−38‰) recorded at the very base. In marked contrast, $\delta^{15}N$ shows an overall progressive decreasing trend from > +4‰ at the base to < +1‰ at the top of the lower unit.

The upper unit corresponds to the upper part of the black shale interval of the Yuertusi Formation (Figure 2). It is distinguished by stable $\delta^{13}C_{org}$ (~−34‰) and $\delta^{15}N$ (~+3‰) values. Notably, $\delta^{13}C_{org}$ in the upper unit is systematically heavier than in the underlying lower unit by ~2‰. TOC remains low and uniform at ~2 wt.% throughout most of the upper unit, before increasing to ~5 wt.% at the top.

5. Discussion

5.1. Preservation of $\delta^{15}N$ signatures

Sedimentary nitrogen exists primarily in two forms: organic-bound nitrogen characterized by relatively consistent C/N ratios, and clay-associated inorganic nitrogen that lacks associated organic carbon (Ader *et al.* 2016; Stüeken *et al.* 2016). The Penglaiba section exhibits a strong linear correlation between TN and TOC, demonstrating that sedimentary nitrogen is mainly sourced from marine organic matter and precluding substantial contributions from exogenous non-primary nitrogen reservoirs (Figure 3A; Calvert 2004). The small positive intercept of this regression line on the TN axis can be attributed to clay mineral scavenging of ammonium (NH_4^+) released during anaerobic microbial degradation of organic matter in early diagenesis (Macko *et al.* 1986).

While primary nitrogen isotope compositions of sedimentary organic matter can be altered during diagenesis, the magnitude of this alteration is strongly modulated by depositional redox conditions. Under oxic bottom water conditions, bulk sediment $\delta^{15}N$ can increase by 3‰–5‰ during diagenesis (Lehmann *et al.* 2002; Prokopenko *et al.* 2006; Robinson *et al.* 2012). In stark contrast, diagenetic processes operating under persistently anoxic conditions induce only minimal nitrogen isotopic fractionation, typically less than 1‰ (Lehmann *et al.* 2002; Thunell *et al.* 2004). Importantly, because diagenetic $\delta^{15}N$ enrichment is directly linked to nitrogen loss from organic matter, cross-plots of $\delta^{15}N$ against TOC, TN, and C/N ratios serve as robust diagnostic tools for assessing the preservation of primary isotopic signatures, with significant correlations in these plots indicative of severe diagenetic overprinting (Ader *et al.* 2014, 2016; Cremonese *et al.* 2014; Chang *et al.* 2019, 2022). Critically, samples from the Yuertusi Formation at the Penglaiba section show no significant correlations in any of these diagnostic cross-plots (Figure 3B–D).

Subsequent metamorphic processes can further modify bulk sediment $\delta^{15}N$ signatures through the volatilization of sedimentary nitrogen, which preferentially releases ^{15}N-depleted NH_3 or N_2 (Ader *et al.* 2014). The magnitude of metamorphic $\delta^{15}N$ alteration is typically < 1‰ below greenschist facies; with increasing metamorphic grade, sedimentary $\delta^{15}N$ values can be altered by 1‰–2‰ at greenschist facies, 3‰–4‰ at amphibolite facies, and up to 6‰–10‰ at upper amphibolite facies (comprehensive review in Ader *et al.* 2016). Detailed field lithological observations confirm that the Yuertusi Formation in our study area is well below greenschist facies metamorphic grade, consistent with results from previous studies (Zhu *et al.* 2024). Consequently, metamorphic modification of the $\delta^{15}N$ signatures in our samples is considered negligible.

Collectively, it is plausible to suggest that the primary sedimentary $\delta^{15}N$ signatures of the Penglaiba section have not undergone significant diagenetic or metamorphic alteration. Therefore, the nitrogen isotope results presented in this study can reliably be used to reconstruct marine redox conditions in the Tarim Basin during the Terreneuvian.

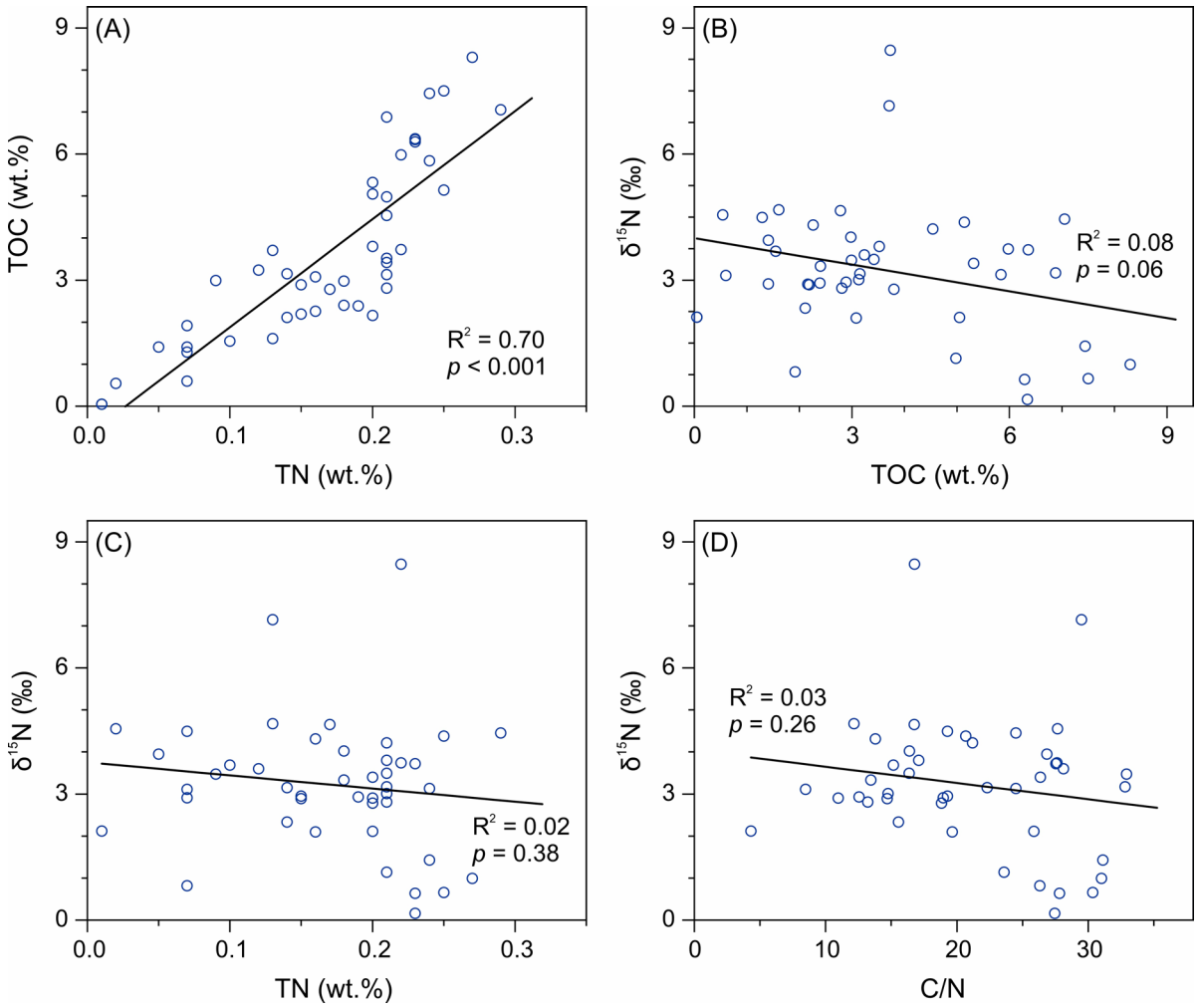

Figure 3. Cross-plots of **(A)** TOC–TN, **(B)** $\delta^{15}N$–TOC, **(C)** $\delta^{15}N$–TN, and **(D)** $\delta^{15}N$–C/N for the Penglaiba section.

5.2. Explanation of $\delta^{15}N$ signatures and redox variations

Sedimentary $\delta^{15}N$ compositions provide a uniquely powerful geochemical tracer for reconstructing nitrogen cycling dynamics in the marine photic zone, given that the vast majority of nitrogen preserved in sedimentary organic matter originates from nitrogen assimilation by photosynthetic primary producers (Stüeken *et al.* 2016). The integrated $\delta^{15}N$ signal exported from the photic zone reflects a balance between the isotopic composition of external nitrogen inputs and the fractionating effects of biogeochemical processes operating within the local water column.

Under conditions of mild water column deoxygenation, bacterial denitrification preferentially removes ^{14}N from the nitrate pool, releasing ^{15}N-depleted N_2 to the atmosphere and enriching the residual dissolved nitrate in ^{15}N (Mode III, Figure 4). As deoxygenation intensifies and denitrification becomes more pervasive, extensive nitrogen loss from the water column leads to severe nitrogen limitation. This nutrient stress triggers a shift in primary producer communities toward diazotrophic cyanobacteria, which fix atmospheric N_2 and produce organic matter with diagnostic near-zero $\delta^{15}N$ signatures (−2‰ to +1‰; Stüeken *et al.* 2016; Mettam and Zerkle 2021). The increasing contribution of diazotrophs to primary production drives sedimentary $\delta^{15}N$ values progressively toward ~0‰ (Mode II, Figure 4; Tyrrell 1999). Under extreme anoxic conditions, the upward expansion of anoxic water masses delivers ^{15}N-depleted ammonium to the photic zone, a process that has been invoked to explain the exceptionally low sedimentary $\delta^{15}N$ values (< −2‰) documented during major oceanic anoxic events in Earth history (Higgins *et al.* 2012; Naafs *et al.* 2019).

In the well-oxygenated modern ocean, the deep ocean contains an enormous nitrate reservoir with a relatively uniform $\delta^{15}N$ value of ~+5‰. Upwelling of this deep-ocean nitrate constitutes the dominant external nitrogen source for surface ocean primary production (Sigman *et al.* 2009). Consequently, modern marine sedimentary $\delta^{15}N$ signatures primarily reflect the degree of nitrate supply from the deep ocean: regions with sufficient nitrate availability exhibit $\delta^{15}N$ values close to the deep-ocean endmember (~+5‰), while regions with limited nitrate supply are characterized by near-zero $\delta^{15}N$ values due to the dominance of N_2 fixation (Tyrrell 1999; Montoya *et al.* 2002, 2004). In stark contrast,

the redox-stratified oceans of the Precambrian lacked a persistent, well-mixed deep-ocean nitrate reservoir, and aerobic nitrogen cycling processes were spatially confined to oxygenated surface waters (Stüeken *et al.* 2024; Chang and Algeo 2025). Under these conditions, sedimentary $\delta^{15}N$ signatures were primarily governed by local or regional water column redox conditions rather than global ocean nutrient cycling, resulting in more significant spatial heterogeneity compared with the modern ocean (Stüeken *et al.* 2013; Chen *et al.* 2019; Chang and Algeo 2025).

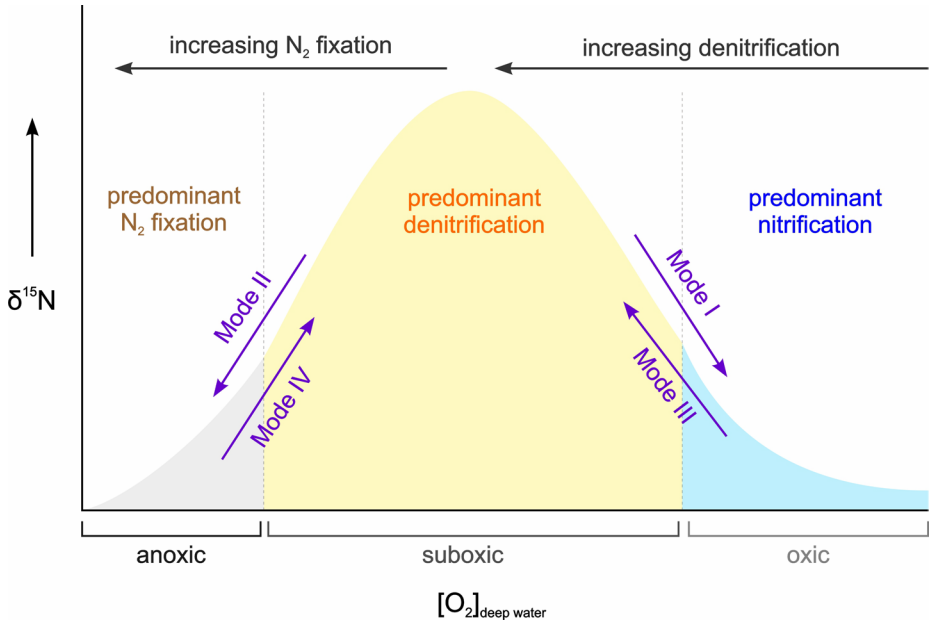

Figure 4. Conceptual model of four sedimentary $\delta^{15}N$ cycling modes as a function of deep-water oxygen levels ($[O_2]$ deep water), after Quan *et al.* (2013) and Chang and Algeo (2025). During oxic-to-anoxic transition, $\delta^{15}N$ first increases via enhanced suboxic water-column denitrification and progressive ^{15}N enrichment of remaining nitrate (Mode III), then decreases as cyanobacterial N_2 fixation is stimulated by severe nitrogen depletion from denitrification (Mode II). The reverse sequence occurs during the transition from anoxic back to oxic conditions (Modes I and IV). Points A–D on the model curve denote relative $\delta^{15}N$ changes under varied redox environments.

As shown in Figure 2, the lower unit of the Yuertusi Formation at the Penglaiba section records a progressive decline in sedimentary $\delta^{15}N$ values, ranging from > +4‰ at its base to < +1‰ at its top. In contrast, the upper unit of the Yuertusi Formation is marked by stable $\delta^{15}N$ values of ~+3‰ (Figure 2). One possible interpretation for this isotopic pattern is that intensified N_2 fixation was stimulated by severe nitrogen depletion driven by water-column denitrification during marine deoxygenation in the lower unit (Mode II, Figure 4), followed by partial marine oxygenation and the re-establishment of incomplete water-column denitrification in the upper unit (Mode IV, Figure 4). Alternatively, the progressive $\delta^{15}N$ decrease in the lower unit could be attributed to diminished water-column denitrification associated with marine oxygenation (Mode I, Figure 4), followed by the re-establishment of incomplete water-column denitrification during marine deoxygenation in the upper unit (Mode III, Figure 4).

Although direct redox constraints from independent proxies are unavailable for this section, systematically lower $\delta^{13}C_{org}$ values in the lower unit relative to the upper unit indicate that the former was most likely deposited under more reducing conditions (Figure 2). This signature is typically linked to enhanced contributions from anaerobic chemoautotrophs, which synthesize organic matter with highly depleted $\delta^{13}C_{org}$ values (Zhang *et al.* 2018; Xiao *et al.* 2017). This interpretation is corroborated by a consistent marine redox history of the Yuertusi Formation in the adjacent Shiairike section, as revealed by integrated nitrogen isotope and elemental redox proxy records (Figure 1; Ju *et al.* 2024; Zhu *et al.* 2024).

Accordingly, the $\delta^{15}N$ increase across the lower–upper unit transition at the Penglaiba section was most likely associated with marine oxygenation (Figure 2), and near-zero $\delta^{15}N$ values at the top of the lower unit reflect near-complete water-column denitrification under highly anoxic conditions (Mode IV, Figure 4). In this framework, the progressive $\delta^{15}N$ decline within the lower unit (Figure 2) is best accounted for by gradual intensification of water-column denitrification during progressive marine deoxygenation (Mode II, Figure 4). This interpretation aligns with the coeval rise in TOC content from ~2 wt.% to ~6 wt.%, given that high-TOC early Cambrian source rocks are generally associated with anoxic depositional settings (Xiao *et al.* 2024; Liu *et al.* 2025).

Spatially, the lower unit of the Yuertusi Formation displays a depth-dependent $\delta^{15}N$ gradient, with values increasing from the deepest basinal setting (Well Tadong 2) through the intermediate middle ramp setting (Shiairike section)

to the shallowest inner ramp setting (Penglaiba sections) (Figure 1 and Figure 5A; Ju *et al.* 2024; Zhu *et al.* 2024). Significantly, a subset of samples from the Shiairike section yields exceptionally negative $\delta^{15}N$ values (< −2‰), a diagnostic geochemical signature for ammonium assimilation by primary producers under conditions of photic zone anoxia (Zhu *et al.* 2024). This spatial pattern cannot be reconciled with a modern-style aerobic nitrogen cycle, where $\delta^{15}N$ variability is primarily controlled by the balance between external nitrate supply and N_2 fixation intensity. Instead, the gradient is most parsimoniously explained by progressively more oxygenated conditions and decreasing degrees of water-column denitrification from basinal to inner ramp facies (Mode IV; Figure 4).

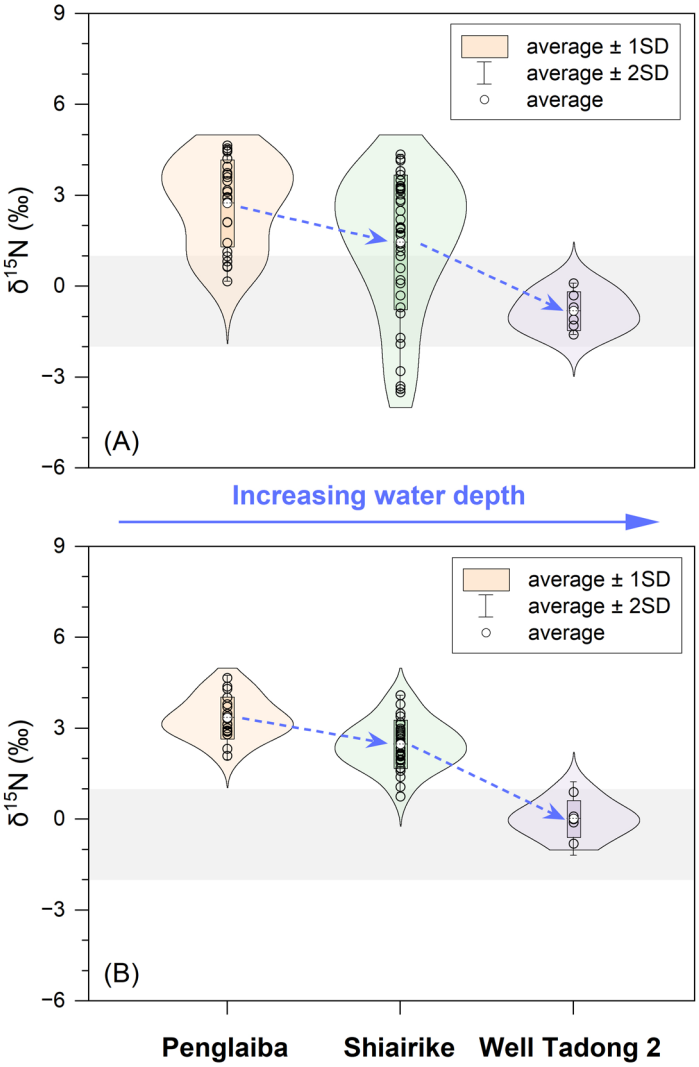

Figure 5. Butterfly distribution plots illustrating spatial distribution of $\delta^{15}N$ values in the low and upper parts of the Yuertusi Formation with increasing water depths from the Penglai through Shiairike to Well Tadong 2 sections. Data for the Shiairike and Well Tadong 2 sections are from Ju *et al.* (2024) and Zhu *et al.* (2024). Stratigraphic correlation of the lower and upper units of the Yuertusi Formation across these sections is established primarily on the basis of their distinct $\delta^{13}C_{org}$ chemostratigraphic signatures. Band widths of the plots reflect the magnitude of the relative distribution frequency. Mean ±1 SD and ±2 SD ranges encompass approximately 68% and 95% of all data points, respectively.

The systematic depth-dependent $\delta^{15}N$ gradient persists into the upper unit (Figure 5B). Although the Penglaiba and Shiairike sections are dominated by positive $\delta^{15}N$ values > +1‰, geochemical evidence from the Shiairike section, including persistent Fe/Al ratios > 0.5 and ferruginous iron speciation, unequivocally demonstrates that the water column remained redox-stratified throughout deposition of the upper unit (Zhu *et al.* 2022; Ju *et al.* 2024). These positive $\delta^{15}N$ values are therefore most parsimoniously interpreted as recording water-column denitrification under suboxic conditions, rather than the development of a fully aerobic nitrogen cycle analogous to that of the modern ocean in the shallow-water inner and middle ramp facies. Under this interpretation, the $\delta^{15}N$ depth gradient reflects increasing degrees of water-column denitrification as conditions transition from suboxic on the inner ramp to anoxic in the deep basin, which is fully consistent with

the persistence of near-zero $\delta^{15}N$ signatures at the Well Tadong 2 section (Figure 5B; Zhu *et al.* 2024).

In summary, our high-resolution $\delta^{15}N$, $\delta^{13}C_{org}$, and TOC records from the Penglaiba section document a two-stage evolution of redox conditions in the early Cambrian Tarim Basin: progressive deoxygenation during deposition of the lower Yuertusi Formation, followed by partial reoxygenation during deposition of the upper unit. When integrated with existing regional $\delta^{15}N$ data, our results demonstrate that a depth-dependent $\delta^{15}N$ gradient, controlled primarily by lateral variations in water-column redox conditions rather than global ocean nutrient cycling, persisted throughout deposition of the Yuertusi Formation.

5.3. Insights into paleoenvironmental and biological co-evolution

The Ediacaran–Cambrian transition witnessed the most dramatic biological radiation in Earth's history, and decades of geochemical research have focused mainly on deciphering the role of marine redox fluctuations in driving the Cambrian Explosion. These studies have revealed highly dynamic changes in the spatial extent of seafloor anoxia and converged on the conclusion that marine redox state exerted an important control on early metazoan evolution. However, significant debate remains regarding the tempo and spatial scale of redox changes, with competing hypotheses emphasizing global ocean oxygenation (e.g., Wen *et al.* 2011; Chen *et al.* 2015), progressive oxygenation of shallow marine environments (e.g., Jin *et al.* 2016; Li *et al.* 2017, 2018), and episodic redox oscillations (e.g., Wei *et al.* 2018, 2021).

Recent advances in nitrogen isotope geochemistry have provided new insights into this debate. Systematic $\delta^{15}N$ studies from the Yangtze Subprovince of South China have documented widespread denitrification across platform facies during the Terreneuvian, indicating that suboxic conditions were pervasive in shallow marine waters at this time (Chang and Algeo 2025; Zheng *et al.* 2025). This stands in stark contrast to Cambrian Age 3, when the exceptionally preserved Chengjiang and Qingjiang biotas are associated with near-zero $\delta^{15}N$ values and minimal trace metal enrichment, signaling a transition to well-oxygenated conditions and greatly reduced denitrification (Hammarlund *et al.* 2017; Chang *et al.* 2022). This temporal pattern is particularly significant because it aligns with the multi-stage evolutionary trajectory of early Cambrian metazoans: the Terreneuvian saw the initial diversification of lophotrochozoans with relatively low oxygen requirements, while Cambrian Age 3 witnessed the explosive radiation of ecdysozoans and deuterostomes, which have substantially higher metabolic oxygen requirements (Zhang and Cui 2016).

Integrated with existing regional datasets, our new $\delta^{15}N$ results from the inner-ramp Penglaiba section provide compelling evidence for a depth-dependent redox gradient in the Terreneuvian Tarim Basin, with suboxic conditions prevailing in shallow marine environments. The Yuertusi Formation at the Aksu area yields abundant small shelly fossils (Qian *et al.* 2000, 2009). Hence, our findings extend the previously documented association between SSFs and suboxic environments from the Yangtze Subprovince to the Tarim Basin (Zheng *et al.* 2025). This cross-basin consistency lends important support to the hypothesis that stepwise oxygenation of the shallow ocean was possibly a primary driver of the multi-phase evolution of metazoans during the early Cambrian (Zhang and Cui 2016). On a related note, our results demonstrate the value of nitrogen isotopes for tracking suboxic environment distributions in the early Cambrian ocean, calling for more systematic $\delta^{15}N$ studies across multiple paleocontinents to build a global understanding of shallow-marine oxygenation and its impact on the Cambrian Explosion.

6. Conclusions

High-resolution $\delta^{15}N$, $\delta^{13}C_{org}$, and TOC records from the Penglaiba section document two-stage evolution of shallow marine redox conditions in the Terreneuvian Tarim Basin. The depositional environment experienced progressive deoxygenation during accumulation of the lower Yuertusi Formation, followed by partial reoxygenation during deposition of the upper unit. Integrated with existing regional $\delta^{15}N$ datasets, our new results demonstrate that a depth-dependent $\delta^{15}N$ gradient persisted throughout deposition of the Yuertusi Formation, indicating decreasing degrees of water-column denitrification as conditions transitioned from anoxic in the deep basin to suboxic on the inner ramp. These findings extend the documented Terreneuvian association between small shelly fossils and suboxic environments to the Tarim Basin, lending support to the hypothesis that stepwise oxygenation of the shallow ocean modulated the multi-phase evolution of metazoans during the Cambrian Explosion.

Data availability statement

All the data are uploaded in the Science Data Bank (Supplementary Table S1, https://doi.org/10.57760/sciencedb.37703).

Declaration of generative AI and AI-assisted technologies

The authors did not use generative AI or AI-assisted technologies in the writing of this manuscript.

Acknowledgments

This study was financially supported by National Key R&D Program of China (Grant 2022YFF0802700), National Natural Science Foundation of China (Grant 42572012), and 111 Project (Grant D17013).

Authors' contribution

Conceptualization, C.C.; methodology, C.C.; investigation, C.C. and Z.W.; resources, C.C.; data curation, S.L. and C.C.; writing—original draft preparation, S.L. and C.C.; writing—review and editing, S.L., Z.W., P.J. and C.C.; visualization, S.L. and C.C.; supervision, C.C.; project administration, C.C.; funding acquisition, C.C. All authors have read and agreed to the published version of the manuscript.

Conflicts of interest

The authors declare no conflicts of interest.

References

Ader M, Sansjofre P, Halverson GP, Busigny V, Trindade RIF, *et al.* Ocean redox structure across the Late Neoproterozoic Oxygenation Event: a nitrogen isotope perspective. *Earth Planet. Sci. Lett.* 2014, 396(1):1–13. DOI: 10.1016/j.epsl.2014.03.042

Ader M, Thomazo C, Sansjofre P, Busigny V, Papineau D, *et al*. Interpretation of the nitrogen isotopic composition of Precambrian sedimentary rocks: assumptions and perspectives. *Chem. Geol.* 2016, 429(46):93–110. DOI: 10.1016/j.chemgeo.2016.02.010

Algeo TJ, Li H. Are South China and North China "blocks" or "cratons"? *Palaeogeogr. Palaeoclimatol. Palaeoecol.* 2026, 683:113464. DOI: 10.1016/j.palaeo.2025.113464

Calvert SE. Beware intercepts: interpreting compositional ratios in multi-component sediments and sedimentary rocks. *Org. Geochem.* 2004, 35(8):981–987. DOI: 10.1016/j.orggeochem.2004.03.001

Chang C, Algeo TJ. Nitrogen cycling and marine redox evolution during the Ediacaran–Cambrian transition. *Global Planet. Change* 2025, 245:104679. DOI: 10.1016/j.gloplacha.2024.104679

Chang C, Hu W, Wang X, Huang K, Yang A, *et al*. Nitrogen isotope evidence for an oligotrophic shallow ocean during the Cambrian Stage 4. *Geochim. Cosmochim. Acta* 2019, 257:49–67. DOI: 10.1016/j.gca.2019.04.021

Chang C, Wang Z, Huang K, Yun H, Zhang X. Nitrogen cycling during the peak Cambrian explosion. *Geochim. Cosmochim. Acta* 2022, 336:50–61. DOI: 10.1016/j.gca.2022.09.013

Chen X, Ling H, Vance D, Shields-Zhou GA, Zhu M, *et al*. Rise to modern levels of ocean oxygenation coincided with the Cambrian radiation of animals. *Nat Commun.* 2015, 6:7142. DOI: 10.1038/ncomms8142

Chen Y, Diamond CW, Stüeken EE, Cai C, Gill BC, *et al*. Coupled evolution of nitrogen cycling and redoxcline dynamics on the Yangtze Block across the Ediacaran-Cambrian transition. *Geochim. Cosmochim. Acta* 2019, 257:243–265. DOI: 10.1016/j.gca.2019.05.017

Cole DB, Planavsky NJ, Longley M, Böning P, Wilkes D, *et al*. Uranium isotope fractionation in non-sulfidic anoxic settings and the global uranium isotope mass balance. *Global Biogeochem. Cycles* 2020, 34(8):e2020GB006649. DOI: 10.1029/2020GB006649

Cremonese L, Shields-Zhou GA, Struck U, Ling H, Och LM. Nitrogen and organic carbon isotope stratigraphy of the Yangtze Platform during the Ediacaran–Cambrian transition in South China. *Palaeogeogr. Palaeoclimatol. Palaeoecol.* 2014, 398(2):165–186. DOI: 10.1016/j.palaeo.2013.12.016

Erwin D, Valentine JW. *The Cambrian Explosion: The Construction of Animal Biodiversity*. Greenwood Village: Roberts and Company, 2013.

Fan H, Fu X, Yang R, Wen H, Hu C, *et al*. Hg isotope evidence for oceanic oxygenation during the Cambrian Explosion. *Geochim. Cosmochim. Acta* 2023, 362:104–114. DOI: 10.1016/j.gca.2023.10.020

Guo Q, Deng Y, Hu J, Wang L. Carbonate carbon isotope evolution of seawater across the Ediacaran–Cambrian transition: evidence from the Keping area, Tarim Basin, NW China. *Geol. Mag.* 2017, 154(6):1244–1256. DOI: 10.1017/S0016756817000206

Hammarlund EU, Gaines RR, Prokopenko MG, Qi C, Hou X, *et al*. Early Cambrian oxygen minimum zone-like conditions at Chengjiang. *Earth Planet. Sci. Lett.* 2017, 475:160–168. DOI: 10.1016/j.epsl.2017.06.054

Higgins MB, Robinson RS, Husson JM, Carter SJ, Pearson A. Dominant eukaryotic export production during ocean anoxic events reflects the importance of recycled NH4+. *Proc. Natl. Acad. Sci. U.S.A.* 2012, 109(7):2269–2274. DOI: 10.1073/pnas.1104313109

Jin C, Li C, Algeo TJ, Planavsky NJ, Cui H, *et al*. A highly redox-heterogeneous ocean in South China during the early Cambrian (~529–514 Ma): implications for biota-environment co-evolution. *Earth Planet. Sci. Lett.* 2016, 44:38–51. DOI: 10.1016/j.epsl.2016.02.019

Ju P, Wang Z, Chang C, Zheng Z, Li R, *et al*. Synchrotron-based P K-edge XANES spectroscopy reveals the transition of phosphorus cycling in the early Cambrian ocean. *Palaeogeogr. Palaeoclimatol. Palaeoecol.* 2024, 655:112506. DOI: 10.1016/j.palaeo.2024.112506

Lehmann MF, Bernasconi SM, Barbieri A, Mckenzie JA. Preservation of organic matter and alteration of its carbon and nitrogen isotope composition during simulated and *in situ* early sedimentary diagenesis. *Geochim. Cosmochim. Acta* 2002, 66(20):3573–3584. DOI: 10.1016/S0016-7037(02)00968-7

Li C, Cheng M, Zhu M, Lyons TW. Heterogeneous and dynamic marine shelf oxygenation and coupled early animal evolution. *Emerging Top. Life Sci.* 2018, 2(2):279–288. DOI: 10.1042/ETLS20170157

Li C, Jin C, Planavsky NJ, Algeo TJ, Cheng M, *et al*. Coupled oceanic oxygenation and metazoan diversification during the early–middle Cambrian? *Geology* 2017, 45(8):743–746. DOI: 10.1130/G39208.1

Li Z, Bogdanova SV, Collins AS, Davidson A, Waele BD, *et al*. Assembly, configuration, and break-up history of Rodinia: a synthesis. *Precambrian Res.* 2008, 160(1):179–210. DOI: 10.1016/j.precamres.2007.04.021

Liu H, Lin C, Wang Y, Zhang D. Temporal and spatial evolution analysis: the early Paleozoic Paleo-Uplifts in the Tarim basin. *J. Earth Sci.* 2012, 23(4):559–581. DOI: 10.1007/s12583-012-0275-0

Liu W, Gao P, Lash GG, Xiao X. Co-evolution of life and environment during the early Cambrian of South China: implications for organic matter enrichment. *Earth Sci. Rev.* 2025, 271:105294. DOI: 10.1016/j.earscirev.2025.105294

Macko SA, Fogel Estep ML, Engel MH, Hare P. Kinetic fractionation of stable nitrogen isotopes during amino acid transamination. *Geochim. Cosmochim. Acta* 1986, 50(10):2143–2146.

Mettam C, Zerkle AL. *Nitrogen Isotopes in Deep Time*. Cambridge: Cambridge University Press, 2021.

Montoya J, Carpenter E, Capone D. Nitrogen fixation and nitrogen isotope abundance in zooplankton of the oligotrophic North Atlantic. *Limnol. Oceanogr.* 2002, 47:1617–1628. DOI: 10.4319/lo.2002.47.6.1617

Montoya JP, Holl CM, Zehr JP, Andrew H, Villareal TA, *et al*. High rates of N2 fixation by unicellular diazotrophs in the oligotrophic Pacific Ocean. *Nature* 2004, 430(7003):1027–1032. DOI: 10.1038/nature02824

Naafs BDA, Monteiro FM, Pearson A, Higgins MB, Pancost RD, *et al*. Fundamentally different global marine nitrogen cycling in response to severe ocean deoxygenation. *Proc. Natl. Acad. Sci. U.S.A.* 2019, 116(50):24979–24984. DOI: 10.1073/pnas.190555311

Prokopenko MG, Hammond DE, Berelson WM, Bernhard JM, Stott L, *et al*. Nitrogen cycling in the sediments of Santa Barbara basin and Eastern Subtropical North Pacific: nitrogen isotopes, diagenesis and possible chemosymbiosis between two lithotrophs (Thioploca and Anammox)—"riding on a glider". *Earth Planet. Sci. Lett.* 2006, 242(1):186–204. DOI: 10.1016/j.epsl.2005.11.044

Qian Y, Feng W, Li G, Yang A, Feng M, *et al*. Taxonomy and biostratigraphy of the early Cambrian univalved mollusc fossils from Xinjiang (In Chinese). *Acta Micropalaeontol. Sin.* 2009, 26(3):193–210.

Qian Y, Yin G, Xiao B. Opercula of hyoliths and operculum-like fossils from the lower Cambrian Yuertus Formation, Xinjiang (In Chinese). *Acta Micropalaeontol. Sin.* 2000, 17:404–415.

Quan TM, Wright JD, Falkowski PG. Co-variation of nitrogen isotopes and redox states through glacial–interglacial cycles in the Black Sea. *Geochim. Cosmochim. Acta* 2013, 112:305–320. DOI: 10.1016/j.gca.2013.02.029

Robinson R, Kienast M, Albuquerque A, Altabet M, Contreras S, *et al*. A review of nitrogen isotopic alteration in marine sediments. *Paleoceanography* 2012, 27(4). DOI: 10.1029/2012PA002321

Shu D, Isozaki Y, Zhang X, Han J, Maruyama S. Birth and early evolution of metazoans. *Gondwana Res.* 2014, 25(3):884–895. DOI: 10.1016/j.gr.2013.09.001

Sigman DM, Karsh KL, Casciotti KL. Nitrogen Isotopes in the Ocean. *Encycl. Ocean Sci.* 2009, pp. 40–54. DOI: 10.1016/B978-012374473-9.00632-9

Sperling EA, Frieder CA, Raman AV, Girguis PR, Levin LA, *et al*. Oxygen, ecology, and the Cambrian radiation of animals. *Proc. Natl. Acad. Sci. U.S.A.* 2013, 110(33):13446–13451. DOI: 10.1073/pnas.1312778110

Sperling EA, Knoll AH, Girguis PR. The ecological physiology of Earth's second oxygen revolution. *Annu. Rev. Ecol. Evol. Syst.* 2015, 46(1):215–235. DOI: 10.1146/annurev-ecolsys-110512-135808

Stüeken EE. A test of the nitrogen-limitation hypothesis for retarded eukaryote radiation: nitrogen isotopes across a Mesoproterozoic basinal profile. *Geochim. Cosmochim. Acta* 2013, 120:121–139. DOI: 10.1016/j.gca.2013.06.002

Stüeken EE, Kipp MA, Koehler MC, Buick R. The evolution of Earth's biogeochemical nitrogen cycle. *Earth Sci. Rev.* 2016, 160:220–239. DOI: 10.1016/j.earscirev.2016.07.007

Stüeken EE, Pellerin A, Thomazo C, Johnson BW, Duncanson S, *et al*. Marine biogeochemical nitrogen cycling through Earth's history. *Nat. Rev. Earth Environ.* 2024, 5:732–747.

Thunell RC, Sigman DM, Muller-Karger F, Astor Y, Varela R. Nitrogen isotope dynamics of the Cariaco Basin, Venezuela. *Global Biogeochem. Cycles* 2004, 18(3). DOI: 10.1029/2003GB002185

Tian L, Cui H, Liu J, Zhang N, Shi X. Early-Middle Cambrian paleogeography and depositional evolution of Tarim Basin (In Chinese). *Oil Gas Geol.* 2018, 39(5):1011–1021.

Tyrrell T. The relative influences of nitrogen and phosphorus on oceanic primary production. *Nature* 1999, 400(6744):525–531. DOI: 10.1038/22941

Wei G, Planavsky NJ, He T, Zhang F, Stockey RG, *et al*. Global marine redox evolution from the late Neoproterozoic to the early Paleozoic constrained by the integration of Mo and U isotope records. *Earth Sci. Rev.* 2021, 214:103506. DOI: 10.1016/j.earscirev.2021.103506

Wei G, Planavsky NJ, Tarhan LG, Chen X, Wei W, *et al*. Marine redox fluctuation as a potential trigger for the Cambrian explosion. *Geology* 2018, 46(7):587–590.

Wen H, Carignan J, Zhang Y, Fan H, Cloquet C, *et al*. Molybdenum isotopic records across the Precambrian-Cambrian boundary. *Geology* 2011, 39(8):775–778. DOI: 10.1130/G32055.1

Xiao S, Bykova N, Kovalick A, Gill BC. Stable carbon isotopes of sedimentary kerogens and carbonaceous macrofossils from the Ediacaran Miaohe Member in South China: implications for stratigraphic correlation and sources of sedimentary organic carbon. *Precambrian Res.* 2017, 302:171–179. DOI: 10.1016/j.precamres.2017.10.006

Xiao W, Cao J, Wang X, Xiao D, Shi C, *et al*. Marine chemical structure during the Cambrian explosion. *Earth Sci. Rev.* 2024, 251:104716. DOI: 10.1016/j.earscirev.2024.104716

Yao J, Xiao S, Yin L, Li G, Yuan X. Basal Cambrian microfossils from the Yurtus and Xishanblaq formations (Tarim, north-west China): systematic revision and biostratigraphic correlation of micrhystridium-like acritarchs. *Palaeontology* 2005, 48(4):687–708. DOI: 10.1111/j.1475-4983.2005.00484.x

Zhang C, Zou H, Li H, Wang H. Tectonic framework and evolution of the Tarim Block in NW China. *Gondwana Res.* 2013, 23(4):1306–1315. DOI: 10.1016/j.gr.2012.05.009

Zhang X, Cui L. Oxygen requirements for the Cambrian explosion. *J. Earth Sci.* 2016, 27(2):187–195. DOI: 10.1007/s12583-016-0690-8

Zhang X, Shu D. Causes and consequences of the Cambrian explosion. *Sci. China Earth Sci.* 2014, 57(5):930–942. DOI: 10.1007/s11430-013-4751-x

Zhang X, Shu D. Current understanding on the Cambrian Explosion: questions and answers. *PalZ* 2021, 95(4):641–660. DOI: 10.1007/s12542-021-00568-5

Zhang Y, Yang T, Hohl SV, Zhu B, He T, *et al*. Seawater carbon and strontium isotope variations through the late Ediacaran to late Cambrian in the Tarim Basin. *Precambrian Res.* 2020, 345:105769. DOI: 10.1016/j.precamres.2020.105769

Zhang Z, Li C, Cheng M, Algeo TJ, Jin C, *et al*. Evidence for highly complex redox conditions and strong water-column stratification in an early Cambrian Continental-Margin Sea. *Geochem. Geophys. Geosyst.* 2018, 19(8):2397–2410. DOI: 10.1029/2018GC007666

Zhao G, Wang Y, Huang B, Dong Y, Li S, *et al*. Geological reconstructions of the East Asian blocks: from the breakup of Rodinia to the assembly of Pangea. *Earth Sci. Rev.* 2018, 186:262–286. DOI: 10.1016/j.earscirev.2018.10.003

Zheng Y, Chang C, Li J, Ding Y, Tang X, *et al*. Coupling of shallow marine redox change and multi-stage animal radiations during the early Cambrian. *Gondwana Res.* 2025, 140:50–59. DOI: 10.1016/j.gr.2025.01.003

Zhu B, Li X, Ge L, Chen Y. Nitrogen isotope stratigraphy of the Early Cambrian successions in the Tarim Basin: spatial variability of nitrogen cycling and its implication for paleo-oceanic redox conditions. *Acta Geochim.* 2024, 43(4):785–801. DOI: 10.1007/s11631-024-00681-7

Zhu B, Yang T, Wang J, Chen X, Pan W, *et al*. Multiple controls on the paleoenvironment of the early Cambrian black shale-chert in the northwest Tarim Basin, NW China: trace element, iron speciation and Mo isotopic evidence. *Mar. Pet. Geol.* 2022, 136:105434. DOI: 10.1016/j.marpetgeo.2021.105434

Zhu G, Li T, Zhao K, Li C, Cheng M, *et al*. Mo isotope records from Lower Cambrian black shales, northwestern Tarim Basin (China): implications for the early Cambrian Ocean. *GSA Bull.* 2021, 134(1–2):3–14. DOI: 10.1130/B35726.1

Zhu M, Babcock LE, Peng S. Advances in Cambrian stratigraphy and paleontology: integrating correlation techniques, paleobiology, taphonomy and paleoenvironmental reconstruction. *Palaeoworld* 2006, 15(3):217–222. DOI: 10.1016/j.palwor.2006.10.016